EPJ Web of Conferences **89**, 02002 (2015)
DOI: 10.1051/epjconf/20158902002

Atmospheric monitoring in H.E.S.S.

J. Hahn[a] and R. de los Reyes[b]

Max-Planck-Institut für Kernphysik, PO Box 103980, 69029 Heidelberg, Germany

Abstract. Instruments applying the IACT method, such as H.E.S.S. (High Energy Stereoscopic System), observe VHE (very high energy, $E > 100$ GeV) photons indirectly, using the Earth's atmosphere as a calorimeter. In the H.E.S.S. data reconstruction, the properties of this component are estimated by Monte Carlo simulations of a yearly averaged atmosphere density profile. Deviations of the real atmospheric conditions from this assumed atmospheric model will result in a biased reconstruction of the primary gamma-ray energy and thus the resulting source spectrum. In order to keep the corresponding systematic effects to a minimum, H.E.S.S. operates a set of atmospheric monitoring devices that allows it to characterise the atmospheric conditions during data taking. This information in turn is then used in data selection. Here, a short overview with respect to their usage during source observation and a posteriori analysis data selection will be presented.

1. Introduction

In recent years, observations with Imaging Atmospheric Cherenkov Telescopes (IACT) have opened up a new window to the non-thermal universe, leading to the discovery more than a hundred sources in the VHE band. The reconstruction of gamma-rays in this method is based on the proper understanding and characterisation of Extended Air Showers (EAS) that VHE gamma-rays create in the upper atmosphere. These showers are observable via the Cherenkov radiation the secondary particles emit. It is intuitively clear that a good understanding of the atmosphere, which acts as the calorimeter of the system, is of paramount importance for the IACT method. This is especially true for the reconstruction of source spectra. That is, the light yield of an EAS is roughly proportional to the gamma-ray initial energy. Light absorbers may decrease the light yield and thus cause a systematic bias towards lower reconstructed gamma-ray energies. This in turn may yield to an underestimated flux normalisation of the emission from a given source. Furthermore, if an atmospheric absorber is situated at the height of the shower itself, it might distort its observed shape and thus impact also other reconstructed parameters, like e.g. the direction of the gamma ray.

An array of atmospheric monitoring instruments is installed on the H.E.S.S. site in order to allow for a proper characterisation of the atmosphere above the instrument. In the following, the individual instruments will be presented. Furthermore, the application of atmospheric monitoring data in data quality selection and observation scheduling will be discussed in Sects. 8 and 9. An overview over studies where atmospheric monitoring has been applied in data correction will be given in Sect. 10.

2. The H.E.S.S. telescopes

H.E.S.S. is a stereoscopic system consisting of five imaging atmosperic Cherenkov telescopes (IACT), situated in the Khomas highlands of Namibia (23° 16' 18" South, 16° 30' 00" East). The system is located at 1800 meters above sea level. The four H.E.S.S. phase I telescopes are arranged in a square of 120 side length, with the large H.E.S.S. II telescope at its centre.

2.1 H.E.S.S. phase I

The four initial H.E.S.S. telescopes were commisioned between the years 2002–2003, with the array becoming fully operational in December 2003. These telescopes are of identical design (described in more detail e.g. in [2]), with a dish radius of 13 m, corresponding to a mirror area of 107 m^2, and a field of view of 5°. Each telescope is equipped with 960 Photonis XP2960 photo-multipliers that are operated with fast electronics, allowing it to trigger on pixel coincidences on the nano-second scale which is necessary to isolate Cherenkov light flashes emitted by the air showers from the night sky background (NSB). A central trigger system [3] guarantees that data read-out from the four telescopes is only initiated upon triggering at least two telescopes within a time window of 80 ns. This prevents the read-out of background events triggered by the NSB and therefore decreases the telescope dead-time. In turn, this allows it to decrease the energy threshold of the instrument, which for H.E.S.S. phase I is at about 200 GeV. While the primary purpose of the telescopes is obviously the detection of VHE gamma-rays, they are also used in atmospheric monitoring. That is, the central trigger rate reflects the measured cosmic ray (CR) rate. Assuming the real CR rate is constant, deviations in the central trigger rate are due to a reduced trigger efficiency by both hardware-related and atmospheric effects.

2.2 H.E.S.S. phase II

The 26th of July 2012 was the date of first light of the new 28 m H.E.S.S. telescope which is optimised for observations at lower energies than the H.E.S.S. phase I telescopes. This instrument stands an impressive 50 m tall when pointing at zenith. The field-of-view of the

[a] e-mail: Joachim.Hahn@mpi-hd.mpg.de
[b] e-mail: Raquel.de.los.Reyes@mpi-hd.mpg.de

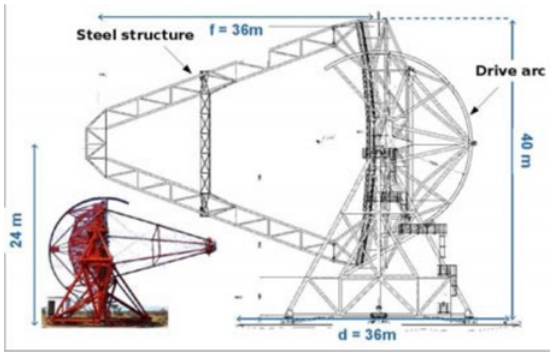

Figure 1. Sketches of a H.E.S.S. phase I telescope and the new large telescope. Taken from [1].

instrument is 3.5° and large light collection area together with the 2048 photo-multipliers installed in the camera result in an energy threshold of 50 GeV when operated alone. This instrument can also be operated together with the H.E.S.S. phase I telescopes, which increases the sensitivity of the array by roughly a factor of 2 and features an energy threshold to a typical value of 80 GeV.

3. The weather station

At the H.E.S.S. site a weather station from Campbell Scientific is present. It allows for the continuous measurement of atmospheric pressure, wind speed and direction, relative humidity, precipitation and air temperature.

The recorded data are fed into the data aquisiton of the H.E.S.S. array and are thus easily accessible to determine the basic atmospheric conditions on site during any given observation.

4. The radiometers

The H.E.S.S. instrument is equipped with five radiometers of the type Heitronics KT19.82 IR. Four of the radiometers are mounted on the H.E.S.S. phase I telescopes, pointing in observational direction. The fifth is operated at the weather station on a rotating mount, performing a full scan of the sky every 30 minutes. These devices feature a 2° field-of-view and operate in the (8–14) μm IR band. They measure the sky radiance, interpreted as a sky temperature using the Stefan–Boltzmann law. Clouds and water vapour appear as especially warm components in the sky and are thus detectable with this kind of instrumentation.

Recent studies have shown that the H.E.S.S. radiometers feature a sensitivity that allows them to measure the increase in bolometric sky luminosity due to atmospheric aerosols [4]. As will be displayed later, the so derived aerosol load measurements correlate well with independent measurements.

5. The ceilometer

From 2002 to 2007 a Vaisala CT25K ceilometer has been operated on the H.E.S.S. site. It applied a InGaAs diode Laser at a wavelength of 905 nm which is well outside the Cherenkov light window and thus allowed for simultaneous operation. The device was able to record atmospheric extinction profiles up to a height of 7 km.

The data were used to spot incoming clouds and to locate low-level aerosol layers. Furthermore, they were used in a detailed atmospheric study [5], see Sect. 10.

6. The lidar

At a distance of 850 m from the H.E.S.S. facilities, the H.E.S.S. LIDAR telescope is located. It features a 60 cm mirror in a Cassegrain configuration and is mounted on a alt-azimuth frame, allowing it to point at any sky position. The laser is situated at a distance of 43 cm to the optical axis of the telescope and is of the Nd:YAG type which operates at the 355 nm and 532 nm wavelength, well overlapping with the Cherenkov light spectrum (∼300–650 nm).

The system is set up in a coaxial configuration and installed in a 5×5 m hut with motorised roof. In order to avoid light contamination, it records atmospheric extinction profiles up to 20 km height only in between observation runs performed by the H.E.S.S. telescopes. The obtained atmospherical profiles may be used to identify and quantify the presence of atmospheric absorbers such as clouds, haze and aerosols. A detailed description of the instrument is given in [6].

7. The atom all-sky camera

Additional to the IACTs, an optical 75 cm telescope is installed at the H.E.S.S. site that is used to monitor observed VHE sources in the optical. Since this telescope, ATOM [7], is operated in a fully automated manner, an automatic protection against rain is necessary. In order to predict rainfall ahead of time, an all-sky camera is installed at the ATOM shelter and used as an atmospheric monitoring device. This camera is equipped with a low-resolution sensor of 640x480px and a fish-eye optics, taking an all-sky image in three minute intervals.

From these images, the positions of up to 5th magnitude stars are extracted and compared to the theoretical expectations derived from a night sky model. The absence of observed stars is then interpreted as a presence of clouds.

8. Data quality selection in H.E.S.S.

In H.E.S.S., the atmospheric monitoring data are used in an automated data quality (DQ) selection mechanism. That is, observational data are checked for hardware and weather criteria. If an observational data set passes both hardware and weather checks, it is flagged as being of "spectral" quality, indicating that atmosphere-induced biases on reconstructed spectral parameters do not lead to systematic errors larger than 20% (see [8]).

However, if only the hardware but not the weather criteria are fulfilled, the data set is flagged as "detection"

Figure 2. The H.E.S.S. array with the four H.E.S.S. phase I telescopes and the new large telescope in the centre.

Figure 3. Picture showing the Ceilometer (left, this device is no longer on site), the weather station (right) and the scanning radiometer (in front of the weather station).

Figure 4. The Heitronics KT19.82 IR radiometer. Five of these devices are operated on the H.E.S.S. site for monitoring primarily clouds and aerosols.

Figure 5. Picture showing the H.E.S.S. LIDAR at night in the shelter with the roof opened. Courtesy of George Vasileiadis.

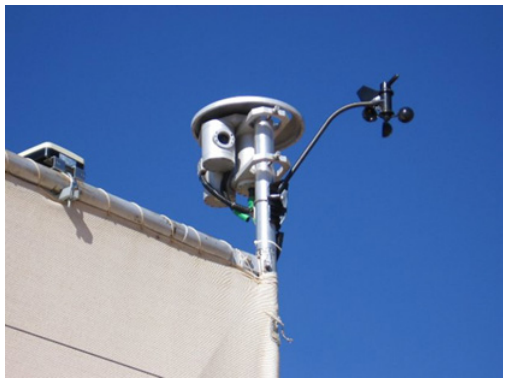

Figure 6. The ATOM all-sky camera, mounted on the ATOM shelter building. Courtesy of Felix Jankowski.

quality, and is not used for spectral analysis. Since typically the main effect of atmospheric attenuation of light showers is on the reconstructed energy and only to a lesser extent on the reconstructed shape[1], gamma-hadron separation as well as direction reconstruction of the shower are still reliable. Thus, these data are still suitable for source detection or the creation of sky maps.

Currently, three atmosphere-related quality quantities are applied in the data quality selection scheme, all of which are derived from the H.E.S.S. phase I trigger rates. The first two quantities are calculated from the central trigger rate [3] and quantify its intra-run fluctuations and variation. Fluctuations in the central trigger rate are typically connected to small-scale absorbers like clouds moving through the field of view, while a monotonical decrease in trigger rate during a run may be connected to an in-moving thin, larger-scale cloud layer.

The third atmosphere DQ quantity is the Cherenkov Transparency Coefficient (CTC), introduced in [8]. It is a quantity derived from the telescope read-out rates, their muon efficiencies [9] and camera gains [10]. By including the latter two hardware parameters, it is possible to largely isolate the adverse impact of large-scale atmospheric absorber structures like aerosol layers on trigger efficiency.

The CTC distribution is normalised to peak at a unity, indicating that a value of $CTC = 1$ corresponds to average, rather than ideal, atmospheric conditions. Correlations with independent, contemporaneous aerosol measurement on site have demonstrated the sensitivity of the CTC to aerosols, see Fig. 7. This is also apparent in Fig. 8, where annual decreases during periods of enhanced biomass burning in the southern parts of Africa are visible.

[1] This might not be true for high-altitude absorbers situated near the shower maximum, see e.g. [5].

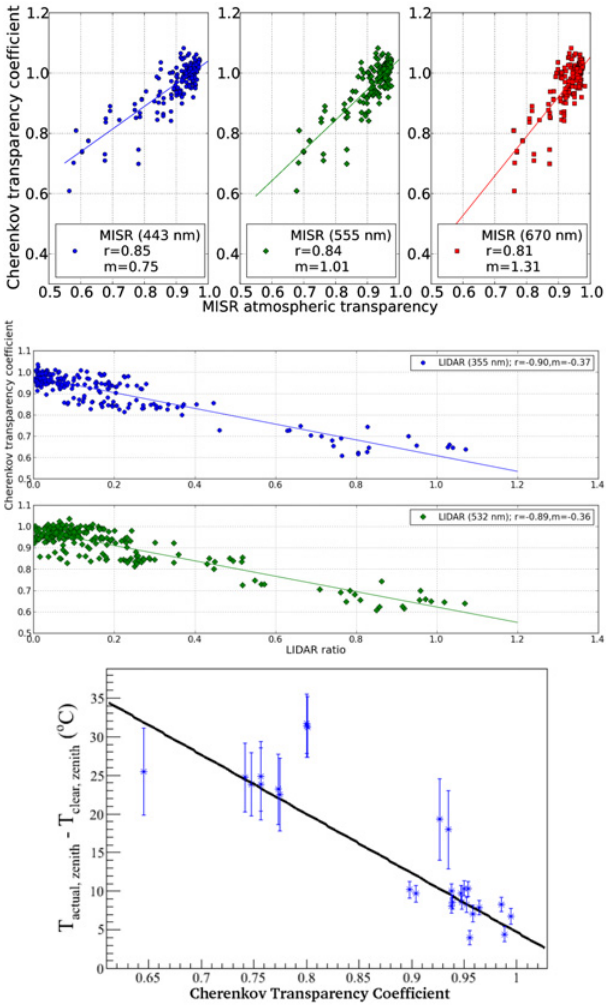

Figure 7. Correlation of the CTC with independent aerosol measurements. Top: correlation with MISR satellite data (taken from [8]), middle: correlation with LIDAR data (taken from [6]), bottom: correlation with radiometer data (correlation factor $r = -0.86$, taken and adapted from [8]).

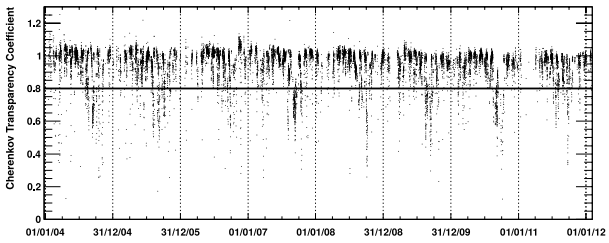

Figure 8. Evolution of the CTC over the last 8 years. The solid line indicates the DQ cut value at 0.8. The distribution is sharply peaked at unity and shows a FWHM $\sim$ 9%. Picture taken and adapted from [8].

9. Smart scheduling in H.E.S.S.

Not all observations require the best atmospheric conditions, for example those where the goal is simply the detection of a source. Contrarily, in those cases where the precise measurement of a source spectrum is desired, any time spent on the object during bad atmospheric conditions is not helpful and could have been spent more efficiently on another source.

In order to make the most efficient use of observational time, a smart scheduling scheme has been implemented in H.E.S.S.. In this scheme, two separate observation schedules are defined for observations that require excellent atmospheric conditions and those that do not. The scheduling scheme processes the radiometer data that are continuously recorded during H.E.S.S. data taking and makes use of the correlation between CTC and sky temperature (see the lower panel of Fig. 7). If the bolometric sky temperature (or to be more precise, the difference between actual and typical sky temperature on zenith) surpasses a value corresponding to a CTC value of 0.7, the telescope operators are informed and have the possibility to switch to the alternative observation schedule optimised for non-optimal atmospheric conditions.

10. Data correction in H.E.S.S.

The ultimate goal in the usage of atmospheric monitoring data is of course not the discarding of data recorded under adverse atmospheric conditions but rather the correction of reconstructional biases.

10.1 Full atmospheric simulations

Such a correction represents a considerable effort: Firstly, there has to be reliable atmospheric monitoring information for every observation. Secondly, a large number of Monte-Carlo simulations has to be performed for various atmospheric conditions in order to provide the proper instrument response functions which then accounts for the atmosphere-induced biases in reconstructed energy and changes to the trigger efficiency.

Such a procedure has been performed and studied by [5], where the authors resurrected bad-weather observational data on the active galactic nucleus PKS 2155-304 that have been taken in 2004.

Using the H.E.S.S. ceilometer, the authors were able to detect an aerosol dust layer of 2 km thickness directly above ground level during several observations. Such a layer can be simulated in the MODTRAN4 *desert* aerosol model with the wind speed as a tuning parameter, which controls the aerosol density. Scanning through this parameter and simulating expected cosmic ray trigger rates with the sim_telarray package in each step, the authors found by comparing to the real trigger rates that the atmospherical conditions could be described by three wind speed classes: 17.5 m/s, 20.0 m/s and 22.5 m/s, where the latter represents the worst atmosphere.

For these three configurations, the authors performed simulations of the H.E.S.S. phase I array and reproduced the appropriate instrument response functions as well as lookup tables required for analysis. By re-analysing the original data, always using the corresponding simulations, it was possible to correct the downward bias in flux normalisation, see Fig. 9.

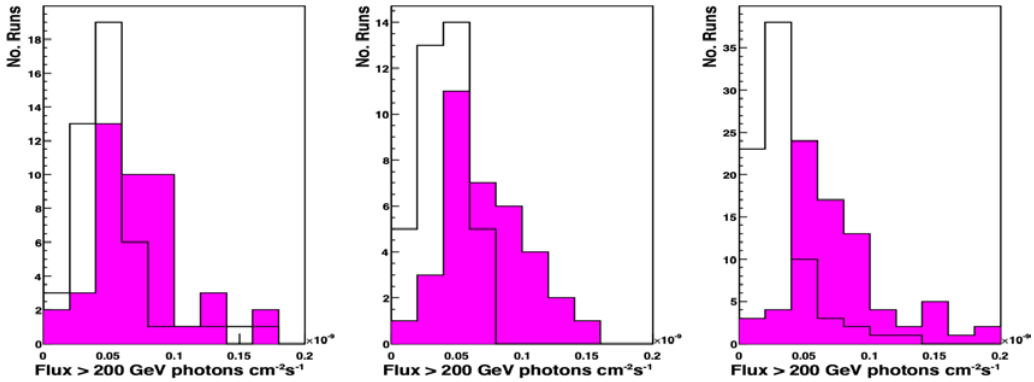

Figure 9. Distribution of integral flux values for individual 28 minute data sets above 200 GeV before (white) and after (magenta) corrections. Left: 17.5 m/s class, middle: 20 m/s class, 22.5 m/s class data. Picture taken from [5].

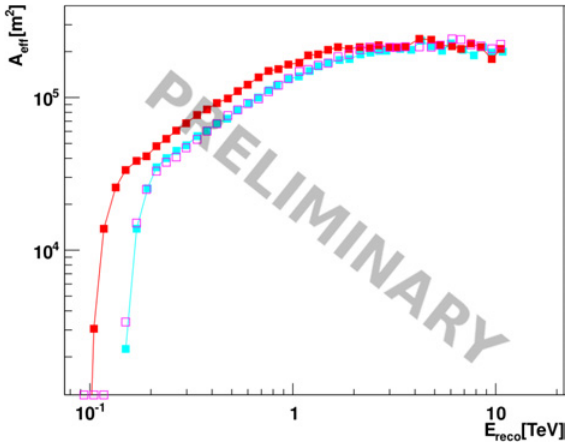

Figure 10. Simulated effective areas in reconstructed energy for PKS 2155-304 observations as described in [5]. Red: good weather, cyan: 22.5 m/s class data. Magenta: effective area resulting from the red data points when correcting the energy according to Eq. (1) and assuming a value of F = 0.7.

10.2 Using the CTC

It was shown in [8] that the reconstructed flux normalisation of the Crab Nebula spectrum follows a power law with the corresponding CTC of the analysed data set. Furthermore, the index of the power-law agrees well with the expectated value that results if one assumes a linear bias in reconstructed energy with the CTC due to atmospheric light attenuation.

In the following, a continuation of this study will be presented, where the suggested CTC dependence is applied in the correction of the reconstructed energy. That is,

$$E_{corr} = E/F(CTC, \theta) \text{ and} \quad (1)$$

$$E_{thr,corr} = E_{thr}/F(CTC, \theta) \quad (2)$$

where E is the uncorrected reconstructed energy of a gamma-ray shower and E_{thr} is the gamma-ray energy threshold[2], which also is assumed to be increased in a linear manner by atmospheric absorption. The CTC is by construction zentith-angle corrected so as to provide an observation-independent atmospheric benchmark quantity. However, in energy correction, the zenith angle correction[3] has to be undone, as one is interested in the actual light absorption in the direction of the source and thus

$$F(CTC, \theta) = CTC^{1/cos(\theta)}$$

is used in Eqs. (1) and (2), where θ is the zenith angle of the observation. Furthermore, one needs an estimate for the effective gamma-ray detection area in the presence of elevated aerosol loads. As has been shown in [5], the effective area in reconstructed energy is shifted towards higher energies under such atmospheric conditions. Here, this shift is emulated by re-assigning an effective area value at energy E to the energy E_{corr} following Eq. (1). This corresponds to a shift of the effective area curve in energy, see Fig. 10.

Correcting the reconstructed energies and safe energy thresholds as well as the effective areas in the described manner, it seems indeed possible to correct the atmosphere-induced biases in the Crab Nebula spectrum, see Fig. 11. There, the total Crab Nebula data set has been divided into three groups: (i) Data that qualify as "detection" quality (see Sect. 8), (ii) data which qualify as "spectral" quality and (iii) an especially strictly selected sample, where the cut on the CTC value has been tightened to $0.95 < CTC < 1.05$. The latter corresponds to data taken under optimal atmospheric conditions. As one can see in Fig. 11, the flux normalisation of the uncorrected data set (i) (red) is heavily biased towards lower values compared to what is found for both the (ii) and (iii) data (green and black, respectively). Upon correcting the energy and effective area for data set (i), this bias is largely removed (blue). In fact, the results that are even closer to that from (iii) than what is obtained from (ii).

Fitting the spectra with a straight power law above 0.51 TeV results in the parameter correlation shown in the bottom panel of Fig. 11. It can be seen that after the correction, the results from data sets (i) and (iii) agree within the 1σ intervals.

[2] Defined as the energy, where the bias in reconstructed energy of the gamma-ray drops below 10%.

[3] Which is a polynomial fit to the telescope read-out rates in $cos(\theta)$.

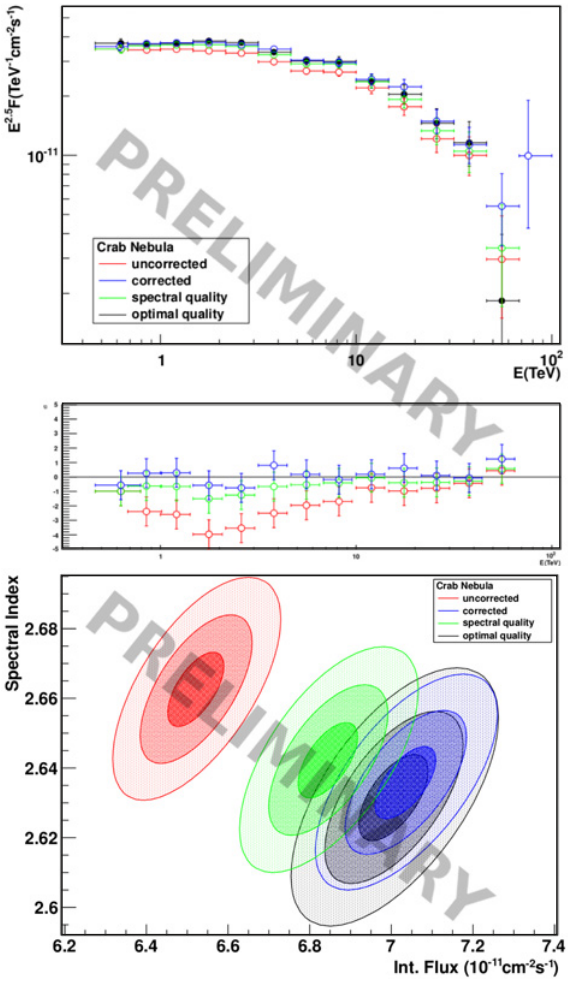

Figure 11. Results of the energy correction using the CTC on the reconstructed Crab Nebula spectrum. Top: differential flux spectrum, middle: flux residuals relative to the "optimal quality" data set, bottom: error ellipses on the power-law best fit values. See text for details.

11. Conclusions

A good understanding of the atmosphere is of central importance in the IACT method, as it plays the role of the calorimeter in the instrumental set up. Motivated by this circumstance, a whole array of atmospheric monitoring devices is operated at the H.E.S.S. site, observing the sky from infra-red to ultra-violet wave-lengths. Some of this information is used in data quality selection to limit biases in reconstructed spectral parameters induced by light attenuation due to atmospheric absorbers. Furthermore, it is now also being applied in a smart scheduling scheme that allows for the most efficient use of observational time. The ultimate goal, however, is to reach an understanding of atmosphere and instrument that makes it possible to correct the mentioned atmosphere-induced biases in reconstructed spectral parameters rather than to discard affected data. To that end, a sophisticated study involving full simulations of atmosphere and instrument has been successfully performed and resulted in the retrieval of bad-atmosphere data taken on the active galactic nucleus PKS 2155-304. A recent study investigating the possibility to correct reconstructed gamma-ray energies with the CTC also yielded encouraging results, as it was possible to correct the biases in flux normalisation and spectral slope of the Crab Nebula spectrum by applying a simple correction scheme. Future work includes the cross-calibration between the atmospheric monitoring devices on site and the continuation and generalisation of the energy correction method involving the CTC. These contributions, as well as the already learned lessons from the atmospheric monitoring with H.E.S.S., will be of great value for the future Cherenkov Telescope Array as they will help to minimise systematic errors induced by atmospheric effects.

References

[1] Becherini, Y. and Punch, M. for the H.E.S.S. collaboration, 2012, AIP Conference Proceedings 1505, 741 (2012)
[2] Aharonian, F. et al., 2006, *A&A* **457**, 899–915
[3] Funk, S. et al., 2004, *Astropart. Phys.* **22**, 285–296
[4] Daniel, M.K. et al., 2013, Proceedings of the Atmo-HEAD workshop 2013, eprint [arXiv:1402.4739]
[5] Nolan, S.J. et al., 2010, *Astropart. Phys.*, **34**, 304
[6] Bourgeat, M. et al., 2014, Proceedings of the Atmo-HEAD workshop 2013, eprint [arXiv:1311.3760]
[7] Hauser, M. et al., 2004, *Astronomische Nachrichten* **325**, 659–659
[8] Hahn, J. et al., 2014, *Astropart. Phys.* **54**, 25–32
[9] Bolz, 2004, *Ph.D. thesis*
[10] Aharonian, F. et al., 2004, *Astropart. Phys.* **22**, 109–125